BILINGUAL PUBLISHING CO.
Advances in Modern Oncology Research
doi: 10.30564/amor.v5i2.236

Article

Resveratrol Reduced Silver Nanoparticles for Anti-tumor Therapy

Ernest Musekwa[1] **Anna M.Nyakabau**[2*]

1. Department of Radiology, College of Health Sciences, University of Zimbabwe, Harare, Zimbabwe
2. Ochsner Clinical School, The University of Queensland School of Medicine, New Orleans, Louisiana, USA

***Correspondence Author:** Anna M.Nyakabau, Ochsner Clinical School, The University of Queensland School of Medicine, New Orleans, Louisiana, USA; Email: Amn_nykabau@gmail.com

Abstract: In situ reduction is one of the easiest and most effective methods to prepare noble metal nanoparticles. The study is to trans resveratrol (RES) as the reducing agent, silver nitrate ($AgNO_3$) as the precursor of silver nanoparticles, cetyl trimethyl ammonium bromide (CTAB) as the surfactant and phase transfer catalyst, and silver based nanoparticles (RES-AgNPs) loaded with RES were prepared by in situ liquid phase reduction process. RES-AgNPs with an average particle size of (45.5±2) nm and zeta potential of 21 mV were prepared when $AgNO_3$, RES and CTAB reacted at 1:1:0.5 (40 °C for 13h). The infrared spectrum and ultraviolet absorption spectrum showed that the RES load on the surface of AgNPs reached 0.883 mg/mL. In addition, RES-AgNPs is sensitive to hydrogen peroxide release. When the pH value of the simulated tumor microenvironment was 5.4 and H_2O_2 was 25 μmol/mL, the release efficiency of RES can reach 89%. *In vitro* antitumor effect of RES-AgNPs, which was determined by MTT experiment, showed that compared with RES, AgNPs and RES+AgNPs, the growth inhibition rate of RES-AgNPs (15μg/mL) on MCF-7 cells was increased by 62.6%, 68.2% and 55.1%, respectively. The result reflected the great synergistic killing effect of AgNPs and RES on tumor cells.

Keywords: Resveratrol; Silver nanoparticles; Anti-tumor therapy

Received: 1 March 2019; ***Accepted:*** 16 March 2019; ***Published Online:*** 1 April 2019

1. Introduction

RES is an active non-flavonoid polyphenolic substance extracted from the plant knotweed, peanut, and grape. As a natural antioxidant, RES has antithrombotic properties on anti-cancer, anti-inflammatory and regulating immune function, preventing oxidative damage of various cells and other biological activities. Importantly, the RES have little toxic side effects [1-2]. However, poor water solubility and low bioavailability limit the biological application of RES [3]. Studies have shown that nanocarriers such as nanoparticles, micelles, liposomes, etc. can load RES to form a colloidal solution system with stable thermodynamic properties, thereby improving the distribution of RES in the water environment and enhancing the anti-tumor effect of RES [4]. Helo et al. reported 150 nm nano-graphene oxide as the carrier, the load rate of RES can reach 69.5%, and the growth inhibition rate of MCF-7 cells can reach 90% [5]. Narayanan et al. reported the RES coated with liposomes to inhibit the growth of prostate cancer cells at a rate of 72% [6]. Mohanty et al. used RES to reduce $HAuCl_4$ to obtain RES gold nanoparticles (RES-AuNPs) with an average particle size of 10nm, and mixed it with DOX to get DOX-RES-AuNPs loaded with RES and DOX simultaneously [7]. The viability of glioma cells LN229 in DOX-RES-AuNPs-treated group was only 24% at 14 g/mL,, which was 0.96 times and 0.33 times of that in the RES-AuNPs group and DOX group, respectively. Kumar et al. obtained RES-AuNPs with an average particle size of 26.63 nm on the surface of AuNPs. Cytotox-

icity experiments, which was used lung cancer cell A549 as a model, showed that the cell viabilities of AuNPs and RES were 108 % and 80 %, respectively, while those of RES- AuNPs were only 51% at 10 mol/L [8].

Precious metal silver (Ag) is considered as a kind of suitable material for near-infrared (NIR) light to visible light, which cloud achieve photothermal conversion due to its significant absorption capacity of NIR in the wide spectral range. In tumor treatment, by loading RES or anti-tumor drugs on the surface of silver nanoparticles (AgNPs), it is expected to improve the therapeutic effect through combined administration [9-11]. Shukla et al. prepared RES-AgNPs with an average particle size of 21.1nm, which was used silver nitrate as precursor and RES as reductant and protective agent [12]. Yuan et al. reported AgNPs with an average particle size of 20 nm using RES as reductant and dispersant, and explored the anti-tumor effect of combined administration of 2, 2-difluorouracil nucleoside (GEM) and AgNPs, which GEM as anti-tumor drug model and ovarian cancer cell model A2780 as cell model. The results suggested that the cell inhibition rate (75%) of the combined group (50 nmol/L GEM+50 nmol/L AgNPs) was higher than that of the GEM group (27%) and AgNPs group (23%) [13].

Studies have proved that surfactants have the dual role of dispersant and phase transfer catalyst in the formation of nanoparticles [14-15]. However, in the preparation of RES-AgNPs, there are fewer reports of cationic surfactants as dispersants and phase transfer catalysts. Importantly, there are fewer reports on the evaluation of the inhibitory effects of RES combined with AgNPs on cell proliferation in different types of tumor cell models. Therefore, the study used CTAB as the dispersant and phase transfer catalyst, RES as the reducing agent, and silver nitrate as the precursor. Through single factor experiments and orthogonal design experiments, the best preparation of RES-AgNPs was obtained. Through the size effect of silver nanoparticles and the anti-tumor activity of resveratrol, the inhibitory effect of RES-AgNPs on the proliferation of MCF-7 cells was evaluated.

2. Materials and Methods

2.1 Materials

CTAB was purchased from China National Pharmaceutical Group Reagent Chemical Co., LTD., $AgNO_3$ was purchased Shanghai Institute of Fine Chemical Materials; Sodium borohydride ($NaBH_4$) was purchased from Tianjin Fuchen Chemical Reagent Factory, 3-(4, 5-dimethythiazole-2)-2, 5-diphenyltetrazolium bromide ($C_{18}H_{16}BrN_5S$) was purchased from Alighting Reagent Co., LTD. Dialysis bag (10kDa) was from Shanghai Lvwu Technology Co., LTD. RES was from Shanghai Civic Chemical Technology Co., LTD.); The reagents were all analytically pure.

2.2 Equipment

Carl Zeiss SIGMA scanning electron microscope (SEM, Carl Zeiss SIGMA, USA); ZEN3600 dynamic light scattering (DLS) granulator (Malvern, UK,); Uv-3600 ultraviolet spectrophotometer (Nanjing Huabi Scientific Instrument Co., LTD., China); Tecnai G2F20 field emission transmission electron microscope (TEM, Phatecom, USA); F50 multifunctional marker (Switzerland Tecan Trading Co., LTD.); Tensor27 Infrared Spectrometer (Brock Spectrometers, Inc., USA); PHS-3C pH meter (Shanghai Electronic Scientific Instrument Co., LTD., China); CHA-S air bath thermostatic oscillator (Jiangsu Jintan Honghua Instrument Factory, China). 5415D high-speed refrigerated centrifuge (Eppende GMBH, Germany);

2.3 Synthesis of Materials

0.5mL of $AgNO_3$ (0.01 mol/L) and 5.0 ml, CTAB solutions (0.1 mol/L) were transferred into 100 mL round bottom flask under the dark condition, followed by 13.9 mL ultra-pure water for 10 min, and 0.6 ml and 10 mmol/L $NaBH_4$ solutions were added drop by drop. After the addition, the reaction took 2 h at 20 °C in a water bath to avoid light. The samples were centrifuged at 25°C at 10000 r/min for 10min to collect precipitation. The precipitation was washed with ultrapure water, dispersed by ultrasound for 5min, centrifuging at 10000 r/min at 25°C for 10min, and the precipitation was collected. Then the AgNPs was obtained by repeated washing and centrifugation for 3 times. RES and CTAB were dissolved in 20 mL aqueous solution of 50% ethanol, and 1.0 mol/L of $AgNO_3$ solution was slowly added to the solution. Under constant temperature, the reaction took 20 min to backflow away from light. After the reaction, the samples were centrifuged at 10000 r/min at 25 °C for 10min, and the precipitation was collected and washed with ultra-pure water to remove the excess CTAB. After ultrasonic dispersion for 5 min, the samples were centrifuged at 10000 r/min at 25°C for 10min, and the precipitation was collected for repeated washing and centrifugation for 3 times. The RES were then washed with anhydrous ethanol to remove the unloaded RES. After ultrasonic dispersion for 5min, the RES were centrifuged at 10000 r/min at 25 °C for 10 min, and the precipitation was

10.30564/amor.v5i2.236

collected. The precipitation was repeatedly washed and centrifuged for 3 times to obtain RES-AgNPs.

2.4 Characterization of Materials

Ultra-pure water was used to dilute the obtained nanoparticles to an appropriate multiple, and 2 mL solution was transferred to a DLS analyzer measurement pool. The average particle sizes, particle size distribution and zeta potential of the samples were measured at 25 °C. SEM was used to observe the morphology, monodispersity and size distribution of the samples under 3 kV accelerating voltage. RES-AgNPs was put into a 5 mL centrifuge tube, 2 mL ethanol was added into the tube and ultrasonic was used for 5min. The samples were uniformly dropped on a 400-mesh copper network. TEM was used to observe the sample morphology under 80kV accelerating voltage. Dry sample with KBr quality than mixing and tablet in proportion of 1:100, the Tensor 27 infrared spectrometer in 500 ~ 4000 cm^{-1} wave number representation the infrared spectroscopy characteristic of the samples.

2.5 Determination of RES Loaded

RES standard solution with concentration of 0.0625, 0.125, 0.25, 0.5 and 1.0 $mmol \cdot L^{-1}$ was prepared with anhydrous ethanol as solvent. The absorbance value of the solution was determined by UV-3600 ultraviolet spectrophotometer at 298 nm, with concentration C as the independent variable and absorbance value A as the dependent variable. The standard curve equation fitting the determination results was: A=3.7187+26.2144C, R^2=0.992. The three centrifuge tubes (1.5 mL) were weight, and record the average weight as W_0. The RES-AgNPs samples were dissolved in ethanol, and three 1000 μL sample solutions were accurately transferred into the weighing centrifuge tube. The centrifuge tube was placed in a constant temperature drying oven at 50°C until the solution in the tube was completely dried, and the average weight was recorded as W_t. Average weight of the nano silver sample under test for $\Delta W=W_t-W_0$.

1000 μL of ethanol were added to the centrifuge tube containing the dried sample to completely dissolve the sample. A UV-3600 ultraviolet spectrophotometer was used to measure the absorbance value of the solution at a wavelength of 308nm, and the RES content C ($mmol \cdot L^{-1}$) in the solution was calculated using the standard curve. Equation (1) is used to calculate the RES loading of RES-AgNPs:

$$E = \frac{C \cdot V \cdot 228}{\Delta W}$$

V is the sample solution volume; 228 is the relative molecular mass of RES.

2.6 Responsive Release

The six samples of 5.0 mg nanoparticles were accurately weighed and added into 10 mL test tubes, denoted as group A, B, C, D, E, F and G. Group A, B and C were added with 5mL phosphate buffer solution with pH 5.4, and H_2O_2 concentration was 0, 5 and 25$\mu mol \cdot L^{-1}$ respectively. Group D, E and F were added with 5mL phosphate buffer solution with pH 7.2, and H_2O_2 concentration was 0, 5 and 25$\mu mol \cdot L^{-1}$ respectively. Then, the solution can be moved to ultrasonic dispersion after 5 min in 6 intercept molecular weight for only 10 kDa dialysis bag, then dialysis bag transferred to the corresponding buffer containing 80 mL conical flask. At intervals, 2mL solution was removed from the conical flask and added with 2mL corresponding fresh buffer solution. The absorbance value of the solution was determined at the wavelength of 298nm, and the RES content in the releasing medium was calculated according to the RES standard curve equation.

2.7 Responsive Release

The blank group, RES group, AgNPs group, RES+AgNPs combined administration group and RES-AgNPs experimental group were set on the 96-well plate. 100μL cell suspension and 100μL fresh culture medium were added to the blank group. 8 sample concentrations (5, 10, 15, 20, 25, 30, 35, 40 $\mu g \cdot mL^{-1}$) were designed for the control group, the combined administration group, and the experimental group. 100μL of $5mg \cdot mL^{-1}$ MTT solution were added to each well and incubating for 4h in a 37°C, 5% CO_2 incubator. The MTT solution was decanted, and 100μL of DMSO solution was added to each well to dissolve the formazan. The cell viability were calculated by measuring the absorbance value at 490nm with a microplate reader.

3. Results and Discussion

3.1 Optimum of Materials

In the redox reaction between RES and Ag^+, RES was oxidized to a quinone structure, and Ag^+ was reduced to elemental Ag [16-17]. Because the outer electron arrangement of silver atoms can form a 5sp3 hybrid empty orbital by 4d105s1, and the 4'-carbonyl oxygen atom in the oxidation state RES molecule can provide a lone pair of electrons, forming a coordination bond. Meanwhile, the excessive addition of reducing state RES in the reaction system can also combine with the coordination of silver crystal nucleus through the H_2O_2 atom in the molecule [18].

The formation of RES molecular layer on the crystal core surface not only realized the high-efficiency drug load but also avoided the aggregation caused by collision of AgNPs, effectively maintaining the good distribution of RES-AgNPs on the nanoscale [12,14].

At condition of $n_{CTAB:\ AgNO3}$ = 2, C_{AgNO3} = 0.1 mol ·L^{-1}, T = 50 ° C T = 8 h, the influence on the average particle size of RES-AgNPs as shown in Figure 1A. When $n_{RES:AgNO3}$<1, the concentration of silver atoms (Ag^0) produced by system restoration was low and the number of nucleuses was small. The growth and formation of AgNPs in the crystal nucleus consumed less energy than Ag^0 aggregation to produce new crystal nucleus. Therefore, Ag^0 produced in the system was mainly adsorbed and deposited on the surface of the crystal nucleus, causing the growth of the crystal nucleus. When $n_{RES:AgNO}$=1, the increase of RES promoted the decrease of Ag^0 generated by Ag^+ in the process of explosive nucleation in a short time, consuming a large amount of Ag^+ in the system. The amount of Ag^+ used for the growth of Ag crystal nucleus was reduced, and AgNPs with smaller particle size were easily obtained. Meanwhile, as the number of RES molecules binding to the crystal nucleus increased, the steric hindrance between the particles increased, reducing the particle size to 56.3 nm. When $n_{RES:AgNO3}$>1, the salt saturation of Ag^+ in solution decreased. Nucleation rates of Ag crystal nucleus slowed down, the amount of simple Ag required for crystal nucleus growth increased relatively, and particle size increased, indicating that reducing the concentration of $AgNO_3$ was beneficial to the growth of crystal nucleus. When $n_{RES:AgNO3}$=1, T=50°C, and T= 8h, Figure 1A further showed the impact of $n_{CTAB:AgNO3}$ on average particle size. The results indicated that when $n_{CTAB:AgNO3}$ increased from 0.25 to 1, the average particle size of RES-AgNPs decreased significantly. In the process of nanoparticle formation, CTAB had the dual role of dispersant and phase transfer catalyst. CTAB molecules combined with reducing RES through the hydrophobic chain, carrying them into the aqueous phase from the alcohol phase, which increased the probability of contact between RES and Ag^+ to promote the reaction. After the reaction, the esterophilic end of CTAB was separated from the oxidation state RES, and the catalytic reaction was repeated. At the same time, the combined Ag surface nucleus of the RES molecule also provided the surface adhesion molecules of CTAB, forming an aligned structure of nanoparticles. The directionally aligned nanoparticles and the hydrophilic ends prevented the collision and aggregation of AgNPs. Therefore, it was beneficial for the formation of small-sized nanoparticles to increase the content of CTAB in the reaction system. As the micelle structure around the AgNPs crystals gradually reached a saturated state, and the influence of CTAB content on the size of AgNPs was no longer significant. As shown in Figure 1B, when $n_{RES:AgNO3:CTAB}$=1 and t=8 h, the average particle size of nanoparticles was positively correlated with the reaction temperature T, which was because release of the reaction temperature can speed up the reduction of $AgNO_3$ by RES to generate Ag continuously. Due to the large surface tension of the crystal nucleus in the system, the strong attraction effect made Ag^0 adhere to the crystal nucleus surface, and the crystal nucleus grow up. In addition, temperature increased brownian motion between particles, increasing the probability of agglomeration. Meanwhile, the average particle size of AgNPs decreased first and then increased with the extension of reaction time under the conditions of $n_{RES:AgNO3:CTAB}$=1, T=50°C. At the initial stage of the reaction, the concentration of Ag^0 produced in the system was small, and the number of crystal nucleus was also small. At low concentrations, Ag^0 were more likely to deposit on the surface of the existing crystal nucleus than to form new clusters. The stage was characterized by a small number of particles and a large average size. With the extension of the reaction time, the concentration of Ag^0 increased, and more and more crystal nuclei tend to be formed and reduced in RES. Such a number of Ag^0 on the surface of crystal nuclei were relatively reduced, which was shown as the decrease of the average particle size of nanoparticles. With the further extension of reaction time, the AgNPs concentration increased continuously, and the probability of collision between particles increased [19]. In addition, during the growth of AgNPs particles accompanied by ostwaldripening, Ag^0 dissolved and released by smaller AgNPs re-grew on the surface of larger AgNPs, leading to the increase and homogenization of the average particle size of AgNPs with the prolongation of the reaction time. As the reaction progressed, Ag^+ in the solution was gradually consumed, and the formation rate of Ag^0 slowed down, decreasing the growth rate of crystal nucleus [20].

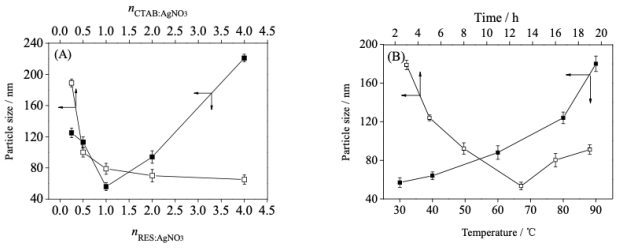

Figure 1. Effects of $n_{RES:AgNO3}$ and $n_{CTAB:AgNO3}$(A), temperature and reaction time (B) on average size of RES-AgNPs

Tumor tissue has the characteristics of abundant blood

10.30564/amor.v5i2.236

vessels and high extravasation, which makes specific size drug-loaded nanoparticles easy to enrich in tumor tissue through the blood circulation system under the enhanced permeability and retention (EPR) effect [21-22]. Studies have shown that nanoparticles with a particle size of less than 100 nm enter cells mainly through endocytosis, and reducing the size of nanoparticles can promote their entry into tumor cells and play a therapeutic role [23-24]. On the basis of single-factor experiments, the experimental results of four-factor and four-level orthogonal design with average particle size as the evaluation index were shown in Table 1. The results showed that the nanoparticles in each experimental group had a small PDI value and particle size distribution range. The order of significance of the influence in the four experimental factors on the average particle size was $n_{RES:AgNO3}$> T > $n_{CTAB:AgNO3}$ > t. The process was optimized, and the conditions for preparing the minimum average particle size AgNPs were $n_{RES:AgNO3}$= 1, $n_{CTAB:AgNO3}$= 0.5, T= 40 °C and t = 13h. Under this condition, the mean particle size of RES-AgNPs was (45.5±2) nm after three repeated experiments.

Table 1. Experimental results and analysis of orthogonal design $L_{16}(4^4)$

	$n_{RES:AgNO_3}$	t / h	T / ℃	$n_{CTAB:AgNO_3}$	Blank	Average size / nm	PDI
1	2	5	40	4	1	125.6	0.151
2	2	8	60	2	2	118.3	0.202
3	2	13	80	1	3	133.5	0.157
4	2	16	90	0.5	4	123.2	0.213
5	1	5	60	1	4	58.9	0.218
6	1	8	40	0.5	3	54.5	0.226
7	1	13	90	4	2	78.3	0.231
8	1	16	80	2	1	82.6	0.165
9	0.5	5	80	0.5	2	73.9	0.175
10	0.5	8	90	1	1	87.5	0.185
11	0.5	13	40	2	4	69.2	0.233
12	0.5	16	60	4	3	65.7	0.187
13	0.25	5	90	2	3	114.3	0.210
14	0.25	8	80	4	4	99.4	0.178
15	0.25	13	60	0.5	1	63.4	0.221
16	0.25	16	40	1	2	56.6	0.138
K_1	125.150	93.175	76.475	92.250	89.775		
K_2	68.575	89.925	76.575	96.100	81.775		
K_3	74.075	86.100	97.350	84.125	92.000		
K_4	83.425	82.025	100.825	78.750	87.675		
R	56.575	11.150	24.350	17.350	10.225		
F	3.523	0.124	0.920	0.329			
Significant		$n_{RES:AgNO_3} > T > n_{CTAB:AgNO_3} > t$					
Optimal level		1	40	0.5	13	45.5	0.261

3.2 Characterization of Materials

The structure and performance of RES-AgNPs were characterized and evaluated by SEM and TEM in Figure 2. The results showed that RES-AgNPs has good sphericity and monodispersity. As shown in Figure 3, The particle size distribution range of RES-AgNPs was 40-50 nm. Compared with AgNPs without RES, the surface potential of RES-AgNPs changed from 8.6 mV to 22.1 mV. The micelle surface layer composed of cationic polar end in CTAB molecule endowed AgNPs with positive surface potential. When RES was loaded on nanoparticles, the partial dissociation of 4 '-phenolic hydroxyl group in the molecules caused RES molecules to carry electronegative oxygen atoms, and the increased absolute surface potential improved the monodispersity of nanoparticles. The infrared spectrometric tests of RES, AgNPs and RES-AgNPs were shown in Figure 4. The ultraviolet absorption spectra of RES, AgNPs and RES-AgNPs were detected. As shown in Figure 5, RES and AgNPs characteristic absorption peaks appeared at 308 nm and 416 nm respectively, indicating that RES was successfully loaded on the AgNPs. During the preparation of RES-AgNPs, the coordination between the oxygen atom in 4 '-phenolic hydroxyl group of RES molecule and a vacant orbital on the Ag^0 on the AgNPs leaded to an increase in the delocalization degree of RES electrons in the RES-AgNPs table, resulting in a decrease in the energy required for electron transition. In addition, the oxidation of 4 '-phenolic hydroxyl in RES molecules was quinone oxygen structure, the increase in the conjugation degree of the oxidation state RES molecules and the increase in the delocalization degree of the RES electrons on the surface that have not been oxidized leaded to the red shift of the characteristic absorption position from 298 nm to 308 nm. Therefore, the absorbance value of RES-AgNPs prepared under the optimal process conditions was measured at 308nm. According to the RES standard curve, the loading amount of RES on AgNPs was calculated to be 0.0883 mg·mg^{-1}.

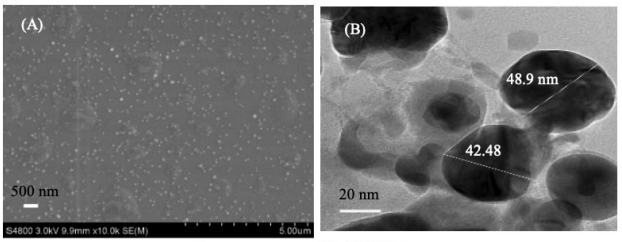

Figure 2. SEM (A) and TEM micrographs (B) of RES-AgNPs

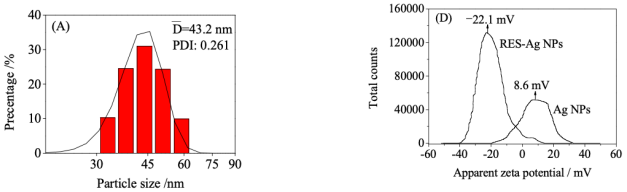

Figure 3. Size distribution (A) and zeta potential values (B) of RES-AgNPs

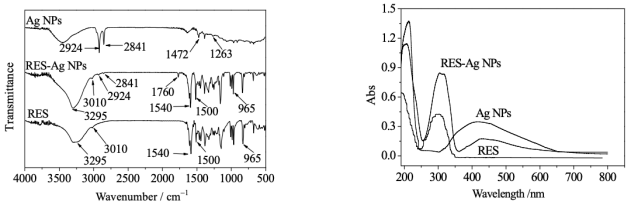

Figure 4. FTIR spectra of RES, AgNPs and RES-AgNPs

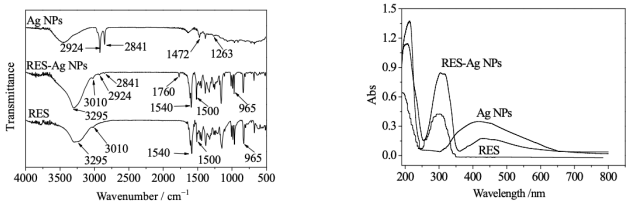

Figure 5. UV absorption spectra of RES, AgNPs and RES-Ag-NPs

3.3 Responsive Release Ability of RES-AgNPs

Studies have shown that When RES-AgNPs enter tumor cells through caveolin-mediated endocytosis, a higher intracellular level' of H_2O_2 can oxidized and release RES [26]. Therefore, H_2O_2 was added to PBS buffer solution with pH=5.4 to simulate the H_2O_2 environment in tumor cells, which was used to study the drug release behavior of RES-AgNPs under the stimulation of environmental factors. As shown in Figure 6, when C_{H2O2} = 0 μmol·L^{-1}, the release rate of RES in RES-AgNPs was only 7.5%. When C_{H2O2} increased to 5 and 25 μmol·L^{-1}, RES release rates reached 77% and 89% within 30 min respectively, showing that the RES-AgNPs has sensitive response to H_2O_2. In addition, in PBS buffer (pH 7.2), when the concentration of H_2O_2 respectively 0, 5, and 25 μmol·L^{-1}, release rates of RES was 3.4%, 37% and 48% within 30 min, and the corresponding indicated that RES-AgNPs was H_2O_2 sensitive response for RES release.

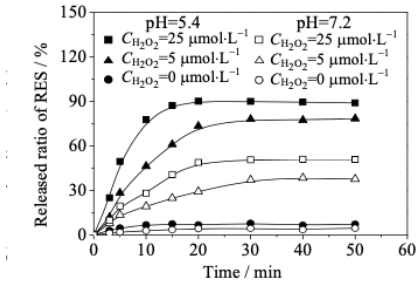

Figure 6. RES release profiles of RES-Ag NPs under hydrogen peroxide and pH stimulation

3.4 Anti-tumor Effect *in vitro*

The MTT method was used to evaluate the killing effect of RES-AgNPs on MCF-7 tumor cells. As shown in Figure 7A, The RES-AgNPs group had a significant dose-dependent effect on the growth inhibition of tumor cells. When the sample dose of each group in the experiment was 15 μg·mL^{-1}, the cell viability of the RES-AgNPs group was 68.2%, 62.6% and 55.1% lower than that of the RES group, AgNPs group and RES+AgNPs combined administration group, respectively; When the sample dose was 40 μg·mL^{-1}, the cell viability of the RES-AgNPS group was 82.2%, 76.8% and 62.5% lower than that of the RES group, AgNPs group and RES+AgNP combined administration group, respectively. Further, as shown in Figure 7B, when the sample dose increased from 5 μg·mL^{-1} to 15 μg·mL^{-1}, cell viability increased from 1.7% to 72.6% in the RES-AgNPs group. However, the cell viability of RES group, AgNPs group and RES+AgNPs combined administration group was only increased by 8.7%, 23.8% and 31.9%, indicating that RES and AgNPs had stronger synergistic killing of tumor cells. Nanoparticles with a particle size of 10-60 nm enter cells mainly through endocytosis. When the amount of nanoparticles is small, the endocytosis rate of nanoparticles is higher than the exocytosis rate. As the dose increased, the ratio of endocytosis and exocytosis approached a balance, resulting in a decrease in cell mortality. Considering the possible risk of cumulative toxicity of high-dose AgNPs to normal tissues and cells, on the premise of ensuring a good killing effect on tumor cells, the appropriate dose of RES-AgNPs was selected as 15g/mL [26-27].

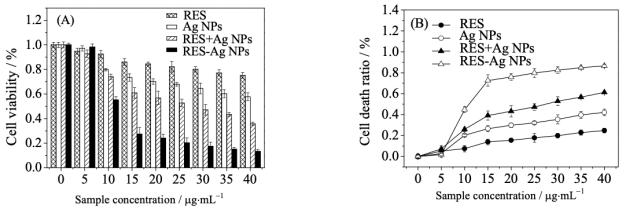

Figure 7. (A) Cell viabilities of RES, AgNPs and RES-AgNPs on MCF-7 cells. (B) Cell death ratio of RES, AgNPs, RES+Ag-NPs and RES-AgNPs on MCF-7 cells

4. Conclusion

In the study, reduction characteristics of RES were used to prepared the resveratrol-loaded AgNPs by liquid-phase reduction method. The prepared RES-AgNPs had good sphericity and uniform particle size distribution. Through single factor experiments, the influence mechanism of the main preparation parameters on the average particle size of RES-AgNPs were analyzed. The preparation conditions were optimized through orthogonal design experiments. When the molar ratio of $AgNO_3$, RES and CTAB was 1:1:0.5 at 40°C for 13 hours, the average particle size was (45.5±2) nm and the RES loading capacity was 0.0883 mg·mg^{-1}. *In vitro* release experiments showed that RES-AgNPs had a faster release characteristic under the simulated tumor environment. MTT experiment results showed that RES-AgNPs had an excellent synergistic killing effect on human breast cancer MCF-7 cells. When the dose of RES-AgNPs was 15μg·mL^{-1}, compared with the RES group, AgNPs group and RES+Ag-NPs combined administration group, the cell death rate of RES-AgNPs group increased strongly.

10.30564/amor.v5i2.236

References

[1] Pangeni R, Sahni J K, Ali J, et al. Resveratrol: review on therapeutic potential and recent advances in drug delivery[J]. Expert Opinion on Drug Delivery, 2014, 11(8): 1285-1298.

[2] Malhotra A, Bath S, Elbarbry F. An organ system approach to explore the antioxidative, anti-Inflammatory, and cytoprotective actions of resveratrol[J]. Oxidative Medicine & Cellular Longevity, 2015, 2015(1-2): 1-15.

[3] Guerrero R F, Garcíaparrilla M C, Puertas B, et al. Wine, resveratrol and health: a review[J]. Natural Product Communications, 2009, 4(5): 635-658.

[4] Hung C F, Chen J K, Liao M H, et al. Development and evaluation of emulsion-liposome blends for resveratrol delivery[J]. Journal of Nanoscience & Nanotechnology, 2006, 6(9-10): 2950-2958.

[5] Hai L, He D, He X, et al. Facile fabrication of a resveratrol loaded phospholipid@reduced graphene oxide nanoassembly for targeted and near-infrared laser-triggered chemo/photothermal synergistic therapy of cancer in vivo [J]. Journal of Materials Chemistry B, 2017, 5(29): 5783-5792.

[6] Narayanan K N. Nargi D, Randolph C, et al. Liposome encapsulation of curcumin and resveratrol in combination reduces prostate cancer incidence in PTEN knockout mice[J]. International Journal of Cancer, 2009, 125(1): 1-8.

[7] Kumar C G, Poornachandra Y, Mamidyala S K. Green synthesis of bacterial gold nanoparticles conjugated to resveratrol as delivery vehicles[J]. Colloids Surf B Biointerfaces, 2014, 123(2): 311-317.

[8] Mohanty R K, Thennarasu S, Mandal A B. Resveratrol stabilized gold nanoparticles enable surface loading of doxorubicin and anticancer activity[J]. Colloids Surf B Biointerfaces, 2014, 114(2): 138-143.

[9] Valodkar M, Jadeja R N, Thounaojam M C, et al. In vitro, toxicity study of plant latex capped silver nanoparticles in human lung carcinoma cells[J]. Materials Science & Engineering C, 2011, 31(8): 1723-1728.

[10] Rajan R, Chandran K, Harper S L, et al. Plant extract synthesized silver nanoparticles: an ongoing source of novel biocompatible materials[J]. Industrial Crops & Products, 2015, 70: 356-373.

[11] Li J, You J, Dai Y, et al. Gadolinium oxide nanoparticles and aptamer-functionalized silver nanoclusters-based multimodal molecular imaging nanoprobe for optical/magnetic resonance cancer cell imaging[J]. Analytical Chemistry, 2014, 86(22): 11306-11311.

[12] Shukla S P, Roy M, Mukherjee P, et al. Size selective green synthesis of silver and gold nanoparticles: enhanced antibacterial efficacy of resveratrol capped silver sol[J]. Journal of Nanoscience & Nanotechnology, 2016, 16(3): 2453-2463.

[13] Park S, Cha S H, Cho I, et al. Antibacterial nanocarriers of resveratrol with gold and silver nanoparticles[J]. Materials Science &Engineering C Materials for Biological Applications, 2016, 58: 1160-1169.

[14] Yuan Y G, Peng Q L, Gurunathan S. Silver nanoparticles enhance the apoptotic potential of gemcitabine in human ovarian cancer cells: combination therapy for effective cancer treatment[J]. Int J Nanomedicine, 2017, 12: 6487-6502.

[15] Starks C M. Phase-transfer catalysis. I. Heterogeneous reactions involving anion transfer by quaternary ammonium and phosphonium salts[J]. Journal of the American Chemical Society, 1971, 93(1): 195-199.

[16] Wright J S, Johnson E R, Dilabio G A. Predicting the activity of phenolic antioxidants: theoretical method, analysis of substituent effects, and application to major families of antioxidants[J]. Journal of the American Chemical Society, 2001, 123(6): 1173-1183.

[17] Zhang X C, Yang Q. Antioxidant effect of resveratrol and its control effect on related diseases[J]. Hans Journal of Food and Nutrition Science, 2017, 06(2): 59-64.

[18] Vongsvivut J, Robertson E G, Mcnaughton D. Surface-enhanced Raman scattering spectroscopy of resveratrol[J]. Australian Journal of Chemistry, 2009, 61(12): 921-929.

[19] Darroudi M, Ahmad M B, Zamiri R, et al. Preparation and characterization of gelatin mediated silver nanoparticles by laser ablation[J]. Journal of Alloys & Compounds, 2011, 509(4): 1301-1304.

[20] Agnihotri, Mukherji S. Antimicrobial chitosan-PVA hydrogel as a nanoreactor and immobilization matrix for silver nanoparticles[J]. Applied Nanoscience, 2012, 2(3): 179-188.

[21] Nakamura H, Jun F, Maeda H. Correction to: development of next-generation macromolecular drugs based on the EPR effect:challenges and pitfalls[J]. Expert Opinion on Drug Delivery, 2015, 12(1): 53-64.

[22] Danhier F. To exploit the tumor microenvironment: since the EPR effect fails in the clinic, what is the future of nanomedicine?[J]. Journal of Controlled Release, 2016, 244(Pt A): 108-121.

[23] Chithrani B D, Chan W C. Elucidating the mechanism of cellular uptake and removal of protein-coated gold nanoparticles of different sizes and shapes[J]. Nano Letters, 2007, 7(6): 1542-1550.

[24] Sakhtianchi R, Minchin R F, Lee K B, et al. Exocytosis of nanoparticles from cells: role in cellular retention and toxicity[J].Advances in Colloid & Interface Science, 2013, 201-202(4): 18-29.

[25] Wlassoff W A, Albright C D, Sivashinski M S, et al. Hydrogen peroxide overproduced in breast cancer cells can serve as an anticancer prodrug generating apoptosis-stimulating hydroxyl radicals under the effect of tamoxifen-ferrocene conjugate[J]. Journal of Pharmacy & Pharmacology, 2007, 59(11): 1549-1553.

[26] Kawata K, Osawa M, Okabe S. In vitro toxicity of silver nanoparticles at no cytotoxicdoses to HepG2 human hepatoma cells[J]. Environmental Science & Technology, 2009, 43(15): 6046-6051.